JCTC Journal of Chemical Theory and Computation

New Investigations of Geometric, Electronic, and Spectroscopic Properties of Tetrapyrrolic Macrocycles by a TD−DFT Approach. Carbon, Nitrogen, and Chalcogen (O, S, Se) Peripheral Substitution Effects on Ni(II) Porphyrazinato Complexes†

Ivan Infante‡ and Francesco Lelj*,§

Faculty of Sciences, Section of Theoretical Chemistry, Vrije Universiteit Amsterdam, De Boelelaan 1083, 1081 HV, Amsterdam, The Netherlands, and LaMI, Dipartimento di Chimica and LaSCAMM, INSTM Sezione Basilicata, Università della Basilicata, Via N. Sauro 85, 85100 Potenza, Italy

Received December 13, 2006

Abstract: The electronic structure of five complexes [M(oXHpz)] [M = Ni^{2+}; oXHpz^{2-} = 2,3,7,8,-12,13,17,18-octakis-substituted (X = CH_2, NH, O, S, Se)-5,10,15,20-tetraazaporphyrinate dianion] has been investigated using a density functional approach. All the geometries have been obtained minimizing the total intramolecular energy using a nonlocal hybrid functional (B3LYP) at the 6-31g* level. The electronic configuration of Ni^{2+} is $(d_{x^2-y^2})^0(d_{xy})^2(d_{xz},d_{yz})^4(d_{z^2})^2$. Optimized geometries exhibit a planar conformation and are all above the threshold for ruffling, which is described by a Ni−N_p bond distance of 1.85−1.87 Å for sterically unhindered porphyrazines. Indeed, the smallest bond distance is 1.880 Å for Ni(oOHpz). Peripheral substituents yield modifications to the "core" of the macrocycle and to the energy levels, changing σ and π interactions. Furthermore, within a time-dependent density functional theory approach, excited states of Ni(oXHpz) [X = CH_2, NH, O, S, Se,] complexes have been studied and compared with available experimental UV−vis spectra.

Introduction

In the past few years, a new challenge for theoretical chemistry has been the possibility to study big systems using massive computational resources. Such large complexes can be now analyzed with full quantum mechanical approaches, like density functional theory, without big loss of accuracy and wasting of time. Furthermore, the contemporary increasing in new techniques to synthesize porphyrazines[1] has provided a new chance to improve the knowledge of these compounds. Indeed, a high growing interest in studying these compounds has been developed because of their high flexibility; rich coordination chemistry; and excellent chemical, thermal, and photochemical stability.[2−21] These new molecules are characterized by a highly delocalized electronic structure in which the four pyrrole moieties are linked to each other by four aza bridges.

Recently, a new branch of compounds has been developed, in which tioether groups are covalently attached at the β positions of the pyrrole moieties.[22−25] These alkyl(sulfanyl)-porphyrazines have interesting spectroscopic and chemical behavior. In particular, transition metal tioether porphyrazines present new in- and out-of-plane peripheral coordination chemistry and have the capability to form liquid crystals and Langmuir−Blodgett films.[26−32] In addition to this, the synthesis of both asymmetric "free-base" and metal ion porphyrazine has become of great interest owing to the formation of a push−pull tetrapyrrolic system lacking a

† Dedicated to Professor Dennis R. Salahub on the occasion of his 60th birthday.

* Corresponding author e-mail: lelj@unibas.it.

‡ Vrije Universiteit Amsterdam.

§ Universita della Basilicata.

10.1021/ct6003609 CCC: $37.00
Published on Web 03/21/2007

symmetry center, which allows these complexes to produce the best performing nonlinear optical materials.[33−35]

One of the main characteristics of porphyrazines, central-coordinated by a nickel ion, is the possibility to easily interchange the peripheral zone of the molecule with different substituents. For example, the syntheses of Ni(oEtpz), Ni(oNH$_2$pz), and Ni(oSCH$_3$pz) have been recently performed, and the closeness on the periodic table of the atoms directly connected to the pyrrole moieties has induced us to explore in more detail the spectroscopic trend along the same row (C, N, O) and the same group (O, S, Se).

The acronym we used to describe the M(oXHpz) porpyrazinato complexes follows these rules: M stands for the metal center in its 2+ oxidation state (Ni^{2+} in this case); o stands for 2,3,7,8,12,13,17,18-octakis-substituted; XH indicates the type of substituents linked to the peripheral pyrroles (X = CH_2, NH, O, S, Se); pz indicates the 5,10,15,20-tetraazaporphyrinate moiety. The whole oXHpz^{2-} is described in its dianionic form.

In this paper, we have studied the electronic structure of Ni(oXHpz) (X = CH_2, NH, O, S, Se) complexes providing deep investigation of the ground and excited states.

In section 2, we have given insights on the methodological approach to compute the properties of the compounds of interest. We elucidated all molecular and electronic properties on the basis of density functional theory.

In section 3, we have analyzed the characteristics of the geometrical structures using peripherally unhindered porphyrazines, in which the terminal atom is simply linked to a hydrogen atom.

In section 4, we have performed an analysis of the soft vibrational modes. We have based our approach on past papers,[36−39] in which it has been shown that possible deformations out of the plane of porphyrin-like molecules can be determined by the peripheral substituents or by the dimension of the "core size". These effects are very interesting because they might provide the modification of redox potential and UV−vis spectra.[40,41] Therefore, we have investigated, analyzing the low vibrational modes, the same characteristics on a peripherally unhindered porphyrazinato complex.

Furthermore, as it can be seen in section 5, the effect of introducing different atoms linked to the four pyrrole moieties is also interesting in the modification of the electronic structure and of the bonding properties. Therefore, we performed calculation using the Ziegler−Rauk fragment decomposition scheme[42,43] to determine the characteristics of the interaction between nickel ions and the porphyrazinato framework. In this scheme, we separate the ionic contribution[44−46] (electrostatic plus Pauli term) and the orbital interactions contribution (σ and π interactions), which is decomposed according to the irreducible representation of the molecular point group.

In section 6, we have coped with the spectroscopic behavior of these porphyrazinato complexes. The spectroscopic behavior of the Ni(oEtpz) complex has been recently investigated in two works. The first explores the nature of the UV−vis bands performing an assignment of the electronic transitions.[47] The spectrum has been shown to be composed by a Q band lying in the visible region and a Soret band, which is characterized by a main band (N) and two shoulders, in the near UV−vis region. It is possible to note a rather small presence in the literature of theoretical works which discuss the issue of the efficacy of different exchange-correlation (xc) functionals on the description of large molecules' excited states such as porphyrazine-like complexes.[48] Furthermore, a deep analysis of the assignment of the transition using different xc functionals (pure and hybrid) has been taken out,[49] in order to figure out how the choice of the functional can produce modification in the nature of the transitions and consequently a different assignment of the electronic excitations.

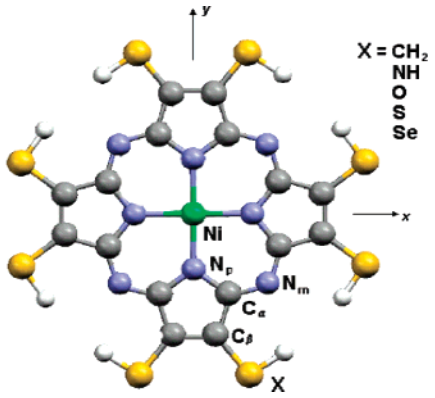

Figure 1. Atom labeling scheme for Ni(oXHpz) [X = CH_2, NH, O, S, Se].

In order to determine from a theoretical point of view the excited states and the oscillator strengths of Ni(oXHpz) [X = CH_2, NH, O, S, Se] complexes, we carried out calculations using time-dependent density functional theory (TD−DFT) (vide infra). This recent method scales with a N^3 factor; therefore, it provides good results with a low computational effort compared to the correlated post-Hartree−Fock procedures. As a first approach (section 6.1), we investigated the effect on the excited states and oscillator strengths induced by the distortion from the planarity of the nickel porphyrazinato complexes. Indeed, the more computationally intensive and the more distorted Ni(oSCH$_3$pz) complex should be taken in consideration because of its larger resemblance with the experimental Ni(oSEtpz) (Et = ethyl) data. In order to avoid too time-consuming calculations, we have underlined the differences with the unhindered Ni(oSHpz) compound, taking the unhindered complex as a reference throughout the paper. In the successive sections (6.2 and 6.3), we analyzed the effect of the peripheral substitution on the transitions and the assignment of these highly delocalized complexes. Section 7 concludes the paper.

2. Computational Details

The electronic structure of Ni(oXHpz) (X = CH_2, NH, O, S, Se) complexes, sketched in Figure 1 together with the reference frame orientation, has been investigated using the Kohn−Sham density functional approach.[50] Geometrical parameters (bond angles and bond distances), low-frequency modes, bonding energies, and excited states have been computed performing a full optimization with strict convergence criteria [4.5 × 10^{-4} for the maximum force and 3.0

Table 1. Geometrical Parameters for Ni(oXHpz) [X = CH_2, NH, O, S, Se] Complexes Calculated at B3LYP/6-31g* Level

bond distance (Å)	X = CH_3	X = NH	X = O	X = S	X = Se
Ni−N_p	1.888	1.880	1.873	1.888	1.890
N_p−C_α	1.375	1.377	1.374	1.375	1.377
C_α−C_β	1.455	1.450	1.450	1.455	1.452
C_β−C_β	1.368	1.370	1.366	1.368	1.364
C_α−N_m	1.319	1.324	1.324	1.319	1.319
C_β−X	1.495	1.393	1.348	1.753	1.878
bond angle (deg)	**X = CH_3**	**X = NH**	**X = O**	**X = S**	**X = Se**
C_α−N_m−C_α	121.4	120.4	119.9	121.4	121.3
C_α−N_p−C_α	105.5	105.1	104.9	105.5	105.6
C_β−C_α−N_p	110.9	111.1	111.3	110.9	110.6
C_β−C_β−C_α	106.4	106.3	106.2	106.4	106.6
C_α−C_β−X	125.7	124.4	124.1	125.7	127.0
C_β−C_β−X	127.9	129.2	129.6	127.9	126.4

$\times 10^{-4}$ for the root-mean square (RMS) of the force] and using as the xc potential the Becke's three-parameter nonlocal hybrid functional (B3LYP)[51] at the 6-31g* basis-set level by the Gaussian 98 package.[52]

All extrema, detected evaluating the matrix of second-derivative energy, have been successively analyzed with the ADF2000 program[53−55] to elucidate the bonding interactions between the metal (Ni^{2+}) and the macrocyclic fragment ($oXHpz^{2-}$) using a Ziegler and Rauk approach.[42,43] In this case, due to technical problems, the xc functional chosen is the GGA Becke−Perdew (BP86).[56] The basis set on metal is an uncontracted triple-ζ Slater-type orbital type augmented by a single-ζ polarization function. A double-ζ plus a single-ζ polarization function has been used for C, N, H, O, S, and Se. The cores of all atoms have been kept frozen.[18]

TD−DFT[57,58] based on the iterative Davidson procedure[59] has been used to determine the excitation energies and oscillator strengths. Transition to the E_u and A_{2u} states are dipole-allowed, and only the former has been analyzed because the oscillator strengths of the latter are too small and not important to the interpretation of the main characteristics of the available experimental spectra (vide infra). In order to evaluate the excitation energies, we have used the Gaussian 98 package using again a B3LYP/6-31g* approach.

3. Molecular Structure

Optimizations using B3LYP/6-31g* yield a good agreement between theory and experiment for the Co(oSHpz) complex;[22] therefore, our studies on Ni(oXHpz) complexes are based on the same approach. Besides, no comparison with experimental geometry is possible lacking, until now, any experimental crystal structure for nickel complexes. Geometrical parameters are described in Table 1. Possible out-of-plane deformations of the macrocycle can be due to two factors: (1) a small ionic radii of the metal, which can contract the "core" (i.e., the M−Np bond distance in this case) and yield a distortion of the planarity and (2) the presence of bulky peripheral substituents. In our study, we consider porphyrazines without peripheral hindrance; that is, only hydrogen atoms are linked to the chalcogen atoms (O, S, and Se; Figure 1). Vibrational analysis on optimized structures shows minima with D_{4h} symmetry for all Ni(oXHpz) [X = CH_2, O, S, Se] molecules, whereas the Ni(oNH_2pz) complex belongs to the D_{2d} point group owing to the rotation of the amine terminal groups to a most stable position. In the latter case, the D_{2d} symmetry is not given by the modification from the planarity but only from the position of the hydrogen atoms in the NH_2 molecule; therefore, the "core" stays planar and the periphery as well. As observed previously, the nonplanar distortions of metalloporphyrins can be classified according to irreducible representations of the D_{4h} point group [D_{2d} for the Ni(oNH_2pz) molecule] of a square-planar porphyrin macrocycle. Extending the same approach to porphyrazines, which have the same porphyrin-like skeleton but with four aza bridges between two adjacent pyrroles, we can classify the lowest-frequency modes in four possible ways: ruf (b_{1u}), sad (b_{2u}), dom (a_{2u}), and wav (e_g) (Figure 2)—as regards the D_{2d} symmetry, we have ruf (a_1), sad (a_2), dom (b_2), and wav (e). In Table 2, the lowest-frequency vibrations are described using a B3LYP/6-31g* approach. No imaginary frequencies are present in the case of planar structures; therefore, all complexes are above the threshold of the ruffling mode, which is described by a Ni−N_p bond distance of 1.85−1.87 Å for sterically unhindered porphyrazines.[40] Indeed, peripheral substitutions with different atoms modify the "core" dimension inducing the shortest Ni−N_p bond distance (1.873 Å) for the Ni(oOHpz) complex and the longest one (1.890 Å) for the Ni(oSeHpz) complex.

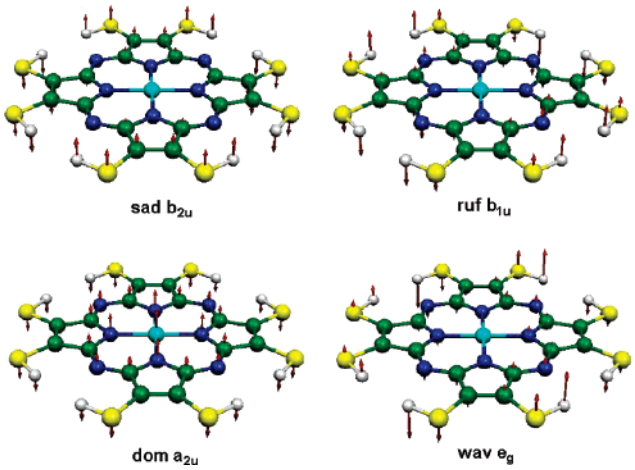

Figure 2. Drawing of the low vibrational out-of-plane modes of Ni(oXHpz) [X = CH_2, NH, O, S, Se] complexes. Arrows' lengths are proportional to the displacement of the eigenvectors.

The different contraction of the "core" induces modifications on the geometrical parameters of the four pyrroles of the macrocycle. In particular, the smallest "core" size for the Ni(oOHpz) complex determines a lowering of the C_α−N_m−C_α bond angle (119.9°) and a stretching of the C_α−N_m bond distance (1.324 Å) with respect to the other three molecules [121.3−121.4° (C_α−N_m−C_α bond angle) and 1.319 Å (C_α−N_m bond distance)], which have about the same "core" size.

Table 2. Low Vibrational Modes (cm^{-1}), Force Constants (mdyn/Å), and Reduced Masses (amu) of Ni(oXHpz) [X = CH_2, O, S, Se] (D_{4h}) and Ni(oNH_2pz) (D_{2d}) Complexes Determined at the B3LYP/6-31g* Level

modes	irreducible representation		Ni(oCH_3pz)	Ni(oNH_2pz)	Ni(oOHpz)	Ni(oSHpz)	Ni(oSeHpz)
saddling	b_{2u}	ν	27	29 (a_2)	32	15	10
		k	0.0019	0.0030	0.0061	0.0021	0.0020
		μ	4.2614	5.9069	10.1932	16.4733	46.7589
ruffling	b_{1u}	ν	32	46 (a_1)	48	26	21
		k	0.0024	0.0070	0.0101	0.0043	0.0101
		μ	4.0267	5.6105	7.4574	10.4722	61.3682
doming	a_{2u}	ν	58	59 (b_2)	55	47	42
		k	0.0092	0.0144	0.0237	0.0273	0.0082
		μ	4.6309	7.0858	13.1603	21.0660	7.8892
waving	e_g	ν	62	83 (e)	84	49	33
		k	0.0024	0.0206	0.0344	0.0150	0.0197
		μ	1.0410	5.0920	8.1184	10.6974	31.3409

4. Analysis of the Low-Frequency Modes

Peripheral unhindered porphyrazines show modes with very low frequencies; thus, we can imagine that the presence of terminal bulky substituents might induce several different modifications from planarity owing to the steric effects between adjacent peripheral tails. The decreasing trend of the frequencies of sad, ruf, dom, and wav modes along the series (O > S > Se) and the increasing trend along the series (C < N < O) might be determined analyzing the force constants and the reduced masses related to these modes (Table 2). We remember that the vibrational frequencies (harmonic approximation) are represented in the following form: $\upsilon = 1.3 \times 10^{-3} \sqrt{k/\mu}$, where ν is expressed in centimeters^{-1}, k is in millidynes per angstrom, and μ is in atomic mass units. From Figure 2, we can note that the sad, ruf, and wav modes are mainly characterized by the vibration of the peripheral atoms. In this way, for the Ni(oOHpz) complex, we obtain the highest force constants (Table 2), probably due to the less polarizable behavior of the oxygen atoms with respect to the sulfur and selenium ones, and intermediate reduced masses, due to the lower atomic weight of the oxygen atoms. The combination of these two factors determines the highest values for the frequencies of the low-frequency modes for Ni(oOHpz). The vibrational gap between the Ni(oSHpz) and the Ni(oSeHpz) complexes are less pronounced, because, in particular for ruf and wav modes, the force constants are smaller in Ni(oSHpz), while the reduced masses are larger for Ni(oSeHpz). In these cases, the reduced masses have a larger impact than the force constants and the molecule with terminal selenium atoms shows the lowest vibrational frequencies. On the contrary, along the CH_3, NH_2, and OH series, the increasing trend can be attributed to the increase of the force constants, because of reduced masses of the same order for the C, N, and O atoms (between 4 and 13 amu).

Different behavior is computed for the doming mode, which is characterized by the out of plane displacement of the "core" atoms (Ni and Np). Also in this case, the Ni-(oSeHpz) complex has the lowest frequency (42 cm^{-1}), but this effect is given by a very low force constant and not by the reduced mass (see Table 2 for further details).

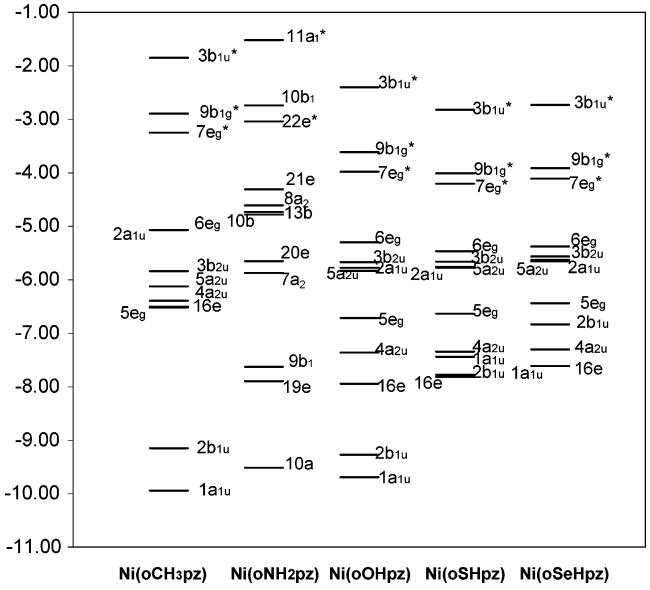

Figure 3. Energy-level diagrams for Ni(oXHpz) [X = CH_2, NH, O, S, Se] complexes at the BP/TZ2P level. All virtual MOs are indicated by a (*) near the labels.

5. Electronic Structure: Ground State

In this paragraph, we used the BP/TZ2P approach to analyze energy levels (Figure 3).

In the previous paragraph, we have seen that the Ni(oNH_2-pz) complex belongs to the D_{2d} point group. This modification of the molecular symmetry is due to the position of the terminal amine groups, which assume their most stable position providing a hydrogen bond between two adjacent NH_2 groups maintaining the σ_h plane. In spite of this lowering of symmetry from D_{4h}, we can observe that the complex is planar and the internal Nipz skeleton (i.e., without the hydrogen atoms linked to the terminal nitrogen atoms) is virtually D_{4h}. Thus, we can compare the molecular orbitals (MOs) obtained for the Ni(oXHpz) [X = CH_2, O, S, Se] complexes with the Ni(oNH_2pz) ones. In this way, we can have the following most important correspondence: $3b_{1u}$-(D_{4h}) → $14a_1$(D_{2d}); $9b_{1g}$ → $11b_1$; $7e_g$ → 23e; $6e_g$ → 22e; $3b_{2u}$ → $9a_2$; $5a_{2u}$ → $13b_2$; $4a_{2u}$ → $12b_2$; $2a_{1u}$ → $10b_1$; $2b_{1u}$ → $12a_1$; and so on.

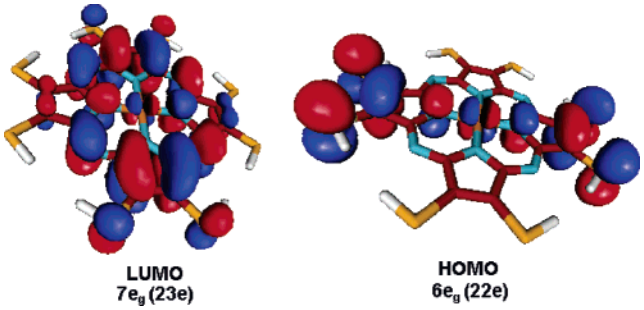

Figure 4. HOMO and LUMO MOs have similar shape for all Ni(oXHpz) complexes. Envelope surfaces at a Ψ value corresponding to 0.02 (1/bohr^3)$^{1/2}$.

As illustrated in Figure 3, peripheral substitution with sulfur atoms yields the lowest highest occupied molecular orbital (HOMO) and lowest unoccupied molecular orbital (LUMO) energies. In all Ni(oXHpz) complexes, the HOMO ($6e_g$) and LUMO ($7e_g$) belong to the same irreducible representation and are characterized by an antibonding π interaction between the d_{xz} (or d_{yz}) atomic orbital and the p_z atomic orbital of nitrogen atoms (Figure 4; see also, Table 3).

The charge rearrangement described by the Mulliken gross population gives only a qualitative understanding of the transfer of electrons between the metal and the ring. In order to analyze from a quantitative point of view the bonding energy, we used the Ziegler and Rauk decomposition scheme described previously.[42,43] The results are reported in Table 4. For a better description of the system, we chose the metal fragment in the +2 oxidation state (Ni^{2+}) with the following electronic configuration of the valence orbitals: $(d_{x^2-y^2})^0(d_{xy})^2(d_\pi)^4(d_{z^2})^2$; while the macrocycle fragment is chosen in the ionic (−2) state ($oXHpz^{2-}$).

5.1. Steric Interaction. The Pauli repulsion term, ΔE^{Pauli}, follows the trend of Ni−N_p bond distances of Ni(oXHpz) complexes, with the most destabilizing term for Ni(oOHpz) being +10.20 eV (Ni−N_p bond distance of 1.873 Å) and with the smallest contribution for Ni(oSeHpz) being +9.51 eV (Ni−N_p bond distance of 1.890 Å). This trend can be explained on the basis of the increase of Pauli repulsion between two closed-shell fragments along with the contraction of the core size.

Amine terminal groups give the most negative electrostatic contribution, ΔE^{elstat}, to nickel porphyrazines [−28.59 eV, against −28.20 eV (X = CH_3), −27.74 (X = O), −25.73 eV (X = S), and −25.03 eV (X = Se)].

In general, the steric interaction ($\Delta E^{Pauli} + \Delta E^{elstat}$) is stabilizing due to the large attractive term, and it follows the trend Ni(oNH_2pz) > Ni(oCH_3pz) > Ni(oOHpz) > Ni(oSHpz) > Ni(oSeHpz).

5.2. Orbital Interaction. The orbital interaction term, ΔE^{oi}, can be decomposed in the irreducible representations belonging to the D_{4h} or D_{2d} point group.

As regards the D_{4h} complexes, the metal does not participate to the a_{2g}, a_{1u}, b_{1u}, and b_{2u} MOs; therefore, their contribution is based only on polarization effects due to the mixing between occupied and unoccupied orbitals of the macrocycle fragment. We aggregated these irreducible representations in a single term denoted ΔE^{nb}, where the subscript nb stands for "nonbonding". The effect is not large though not negligible: −1.54 eV (X = O), −1.56 eV (X = S), −1.57 eV (X = Se), and −1.62 eV (X = CH_2).

The $\Delta E^{A_{1g}}$ term is almost similar in all Ni(oXHpz) complexes, −2.34 eV (X = O, S), −2.35 eV (X = CH_2), and −2.38 eV (X = Se), reflecting an analogous σ donation from the ligand orbitals to the 4s atomic orbital (AO) of the metal.

The $\Delta E^{B_{1g}}$ term is the largest contribution to the orbital σ interaction with a transfer of about one electron to the empty $3d_{x^2-y^2}$ of the nickel atom. Terminal substitution with selenium atoms gives the most stabilizing term [−8.88 eV (X = Se), against −8.81 eV (X = CH_2), −8.60 eV (X = O), −8.63 eV (X = S)].

The $\Delta E^{A_{2u}}$ term gives a little contribution to the π orbital interaction, because the $4p_z$ AO does not have a good match with occupied ligand orbitals. The stabilization is between −0.95 eV (X = O, CH_2) and −1.04 eV (X = S, Se).

The ΔE^{E_u} term is characterized by a strong σ donation from the macrocycle to the $4p_\sigma$ AOs of the metal. In particular, the Ni(oSeHpz) and Ni(oSHpz) complexes show also a polarization effect on the ligand orbitals; therefore, their stabilizations, of −3.78 and −3.57 eV, respectively, are stronger than those of the Ni(oOHpz) and Ni(oCH_3pz) complexes where this polarization is absent.

The $\Delta E^{B_{2g}}$ term gives substantially a nonbonding contribution with a small back-donation from the $3d_{xy}$ AO to the lowest empty ring orbital. The effect is small and similar for all Ni(oXHpz) complexes (between 0.71 and 0.74 eV).

The ΔE^{E_g} term is by far the largest contribution to the π interaction. It is mainly characterized by a π back-donation of almost 0.2 electrons from the d_π AOs of the metal to the ligand virtual orbitals. Previous calculations on the Co(OSMepz) complex,[60] where the polarization prevails over a marginal π back-donation, show how the substitution of the metal center can affect the charge rearrangement between the metal and the tetrapyrrole moiety.

The total orbital contribution prevails over the ionic contribution in all four Ni(oXHpz) complexes. The molecule substituted peripherally with selenium atoms presents the most negative energy: −20.41 eV, followed by Ni(oCH_3pz) [−20.09 eV] ≅ Ni(oNH_2pz) [−20.04 eV] > Ni(oSHpz) [−19.86 eV] > Ni(oOHpz) [−19.64 eV].

As concerns the Ni(oNH_2pz) complex (D_{2d}), the metal contribution is present in all irreducible representations with the exception of the a_2 one. However, this nonbonding contribution is small (1.28) even if not marginal.

Owing to the lowering of symmetry from D_{4h} to D_{2d}, in the ΔE^{A_1} (D_{2d}) term, we can aggregate a bonding $\Delta E^{A_{1g}}$ (D_{4h}) and a nonbonding $\Delta E^{B_{1u}}$ (D_{4h}) contribution. The Ni(oNH_2pz) molecule yields a value (2.43 eV), which is on the same order as those of the other complexes, which are in the range of 2.39−2.51 eV.

The ΔE^{B_1} term can be compared with the sum of $\Delta E^{B_{1g}} + \Delta E^{A_{1u}}$ ones. Also, in this case, the value (8.91 eV) is intermediate with respect to the contributions of the other complexes (in the range between 8.85 and 9.12 eV).

Table 3. Atomic Orbital Contributions (%) for Each Irreducible Representation of Ni(oXHpz) [X = CH_3, O, S, Se] (D_{4h}) and Ni(oNH_2pz) (D_{2d}) Complexes at BP/TZ2P Level

Γ	Ni	L	CH_3	Ni	L	O	Ni	L	S	Ni	L	Se	Γ	Ni	L	NH_2
							Unoccupied Orbitals									
$4b_{2u}$	0	92	8	0	98	2	0	98	2	0	98	2	$10a_2$	0	98	2
$17e_u$	0	4	96	0	8	92	0	8	92	0	8	92	24e	0	8	92
$3b_{1u}$	0	92	8	0	92	8	0	88	12	0	90	10	$14a_1$	0	94	6
$9b_{1g}$	55	41	4	55	44	1	54	44	2	54	42	4	$11b_1$	55	44	1
$7e_g$	4	93	3	4	90	6	4	85	11	4	86	10	23e	4	89	7
							Occupied Orbitals									
$6e_g$	52	44	4	28	50	22	17	49	44	17	35	48	22e	24	61	15
$3b_{2u}$	0	88	12	0	66	34	0	41	59	0	35	65	$9a_2$	0	81	19
$5a_{2u}$	0	86	14	1	60	39	1	35	64	1	29	70	$13b_2$	1	55	44
$2a_{1u}$	0	95	5	0	86	14	0	69	31	0	62	38	$10b_1$	0	92	8
$11a_{1g}$	97	3	0	97	3	0	97	3	0	97	3	0	$13a_1$	97	3	0
$5e_g$	35	54	11	57	25	18	57	15	28	50	13	37	21e	58	47	5
$2b_{1u}$	0	80	20	0	30	70	0	18	82	0	16	84	$10a_1$	2	31	67
$4e_g$	5	91	4	7	74	19	6	24	70	12	20	68	20e	5	54	41
$4a_{2u}$	0	99	1	2	98	0	2	98	0	2	98	0	$12b_2$	1	98	1
$1a_{1u}$	0	12	88	0	23	77	0	41	59	0	46	54	$9b_1$	2	16	82
$16e_u$	0	99	1	0	99	1	0	99	1	0	99	1	19e	0	99	1
$2b_{2u}$	0	66	34	0	63	37	0	66	34	0	69	31	$8a_2$	0	64	36
$3a_{2u}$	0	30	70	0	50	50	1	67	32	0	72	28	$11b_2$	0	32	68

Table 4. Bonding Decomposition Energy (eV) between Ni^{2+} (M) and $oXpz^{2-}$ (L) Fragments for Ni(oXHpz) [X = CH_2, NH, O, S, Se] Complexes According to the Ziegler and Rauk Approach

	Ni(oOHpz)	Ni(oSHpz)	Ni(oSeHpz)	Ni(oCH_3pz)		Ni(oNH_2pz)
Pauli	+10.20	+9.61	+9.51	+9.89	Pauli	+9.96
Elstat	−28.50	−25.77	−25.54	−29.34	Elstat	−28.59
total s.i.	−17.54	−16.12	−15.52	−18.31	total s.i.	−18.63
A_{1g}	−2.30	−2.30	−2.38	−2.35	A_1	−2.43
B_{1g}	−8.60	−8.63	−8.88	−8.81	A_2	−1.28
B_{2g}	−0.75	−0.72	−0.73	−0.75	B_1	−8.91
E_g	−2.13	−2.13	−2.13	−2.05	B_2	−1.78
A_{2u}	−1.03	−0.95	−0.95	−1.04	E	−5.65
E_u	−3.29	−3.57	−3.78	−3.47	total o.i.	−20.04
nb	−1.54	−1.56	−1.57	−1.62	total o.i+s.i	−38.67
total o.i.	−19.64	−19.86	−20.41	−20.09		
total o.i+s. i	−37.18	−35.98	−35.93	−38.39		

The ΔE^{B_2} term is related to the sum of $\Delta E^{B_{2g}} + \Delta E^{A_{2u}}$ ones. The Ni(oNH_2pz) complex provides an orbital interaction (1.78 eV), which is similar to those obtained with the other complexes (between 1.67 and 1.79 eV).

The ΔE^{E} terms can be compared with the sum between ΔE^{E_g} and ΔE^{E_u} terms of the D_{4h} complexes. The total ΔE^{E} contribution (5.65 eV) is on the same order as those of the other porphyrazinato molecules (between 5.42 and 5.92 eV).

5.3. Total Bonding Energy. The total bonding energy ($\Delta E^{si} + \Delta E^{oi}$) indicates that the Ni(oNH_2pz) complex has the strongest $Ni^{2+}/oXpz^{2-}$ interaction, and it is due to the large stabilization energy given by the electrostatic term. In conclusion, the ΔE^{oi} terms are substantially similar for all Ni(oXHpz) complexes. Within the whole set of substituents, its change remains in the range of only 0.8 eV, with respect to the 2.8 eV of the ionic term. Therefore, the total bonding energy is controlled mainly by the steric term, which is the largest for the Ni(oNH_2pz) complex.

6. Electronic Structure: Excited States

The analysis of excitation energies has been performed using the recent TD−DFT approach. This method provides similar results with respect to the post-Hartree−Fock techniques but with a lower computational effort. In particular, Stratmann and co-workers[60] have shown a good agreement between the experimental data and the calculated ones obtained at the B3LYP/6-31g* level on the free-base porphin. Furthermore, we recently analyzed[49] the effect of different xc potentials (B3LYP, BP, BLYP, LB94, and SAOP) on the assignment of the experimental spectrum of the Ni(oEtpz) complex. In that case, the computed RMS, relative to the difference between the calculated and the experimental data, indicates a sufficiently good description provided by the B3LYP/6-31g* approach. The choice of the B3LYP xc functional is not based on a better performance compared to other functionals but on consistency with the rest of the paper. Indeed, despite the overall low RMS, B3LYP does not

describe well the Q region of the spectrum. As regards the choice of the basis set, in a previous paper, it was pinpointed that the excitation energies are substantially unchanged using a basis set as large as 6-311+g**.[61] Therefore, in order to examine the excited states of the Ni(oXHpz) complexes, the B3LYP/6-31g*//B3LYP/6-31g* method has been chosen. All Ni(oXHpz) molecules present a D_{4h} symmetry, with the exception of Ni(oNH$_2$pz) (D_{2d}); therefore, the dipole-allowed transitions belong to the A_{2u} and E_u irreducible representations [B_2, E for the Ni(oNH$_2$pz) complex]. The A_{2u} (B_2) excitations have negligible intensity: the oscillator strengths are on the average 10^3 times less intense than the E_u (E) ones, therefore we will discuss only the E_u (E) transitions. We have also compared our theoretical results with available experimental data.[47,62]

6.1. The Planar Ni(oSHpz) and the Saddled Ni(oSHpz) and Ni(oSCH$_3$pz) Complexes. The first complex analyzed is the Ni(oSHpz) molecule. Indeed, the excited states of the Ni(oHpz) and Ni(oCH$_3$pz) complexes have been recently discussed,[49] and we used their assignment for determining those of the Ni(oXHpz) ones. The TD−DFT results on the Ni(oSHpz) complex are compared with the experimental spectrum collected for the nickel octa(ethyl)sulfanyl porphirazinato [Ni(oSEtpz)] complex in the $CHCl_3$ solvent (Figure 5).

In the visible region is present a main band, denoted as the Q band,[63] which lies at 1.84 eV (673 nm), and it is characterized also by a less intense shoulder (sh_1) at 2.01 eV (616 nm). The second band lies at 2.56 eV (484 nm), and it is denoted as an "extra band". The last band is the Soret band, which lies in the UV region and can be split into several components: the most intense one, that which we denote as the N band, lies at 3.98 eV (311 nm). Furthermore, the spectrum shows significant broadening due to the presence of intermolecular interactions even at a low concentration (1.09×10^{-6} M). As it will be seen soon, the oscillator strengths calculated at the D_{4h} molecular symmetry are too low or too high in intensity with respect to the experimental spectrum. Indeed, the Ni(oSHpz) molecular structure, on which we performed our calculations, is planar, whereas the experimental Ni(oSEtpz) complex might be distorted. Hence, we carried out geometry optimizations on two of the most probable modifications from the planarity of the Ni(oSCH$_3$pz) complex (this complex differs from the unhindered one because we have added methyl groups on the terminal sulfur atoms, and it resembles closely the experimental complex)—the saddled (C_{2v}) and the ruffled (C_{2v}) conformations—and both are more stable than the planar one. The choice of these two isomers is based on the results of the section 4, in which we have pointed out that the two lowest-frequency modes are the sad and the ruf vibrational modes. The first one (sad) has been found more stable of 4.6 kcal/mol than the ruffled one. Therefore, we performed TD−DFT calculations on the saddled Ni(oSHpz) complex (in order to take account of the distortion effects on the excitation energies and oscillator strengths) and on the saddled Ni(oSCH$_3$pz) complex (in order to analyze the methyl substitution effect on the sulfur atoms) (Figure 6). Symmetry lowering from the planar D_{4h} to the distorted C_{2v}

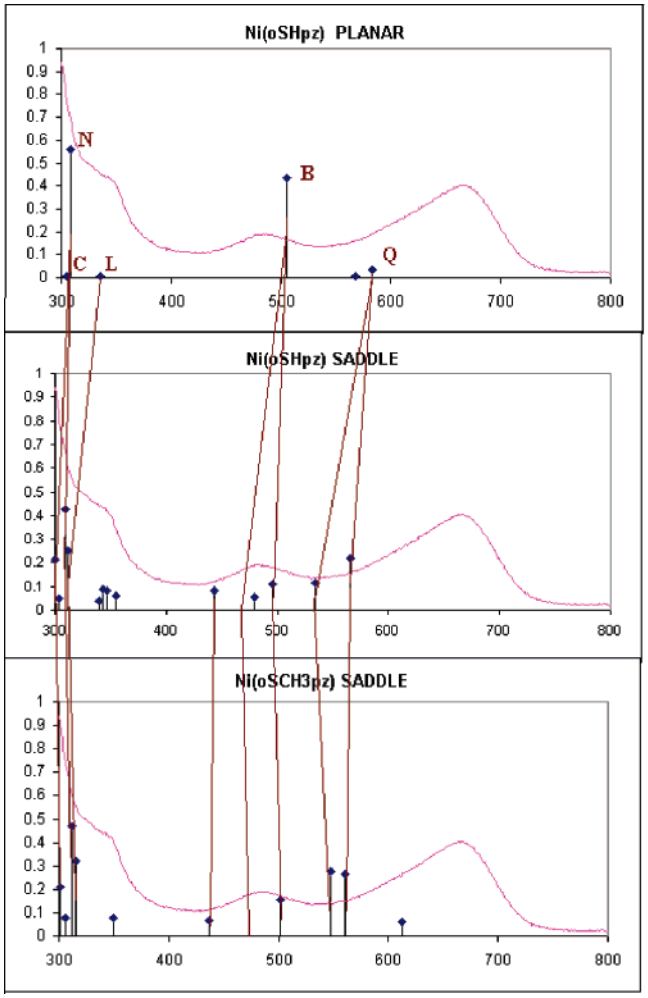

Figure 5. Vertical bold lines indicating the most important calculated singlet−singlet excited states with oscillator strengths higher than 2.5×10^{-2}. The experimental spectrum of the Ni(oSEtpz) complex recorded in a CH_3Cl solution is indicated by a continuum line (—). All the calculations have been performed at the B3LYP/6-31g* level for the Ni(oSHpz) (D_{4h}, C_{2v}) and Ni(oSCH$_3$pz) (C_{2v}).

increases the number of dipole-allowed transitions, though they show low intensities. In order to achieve a straightforward interpretation of the experimental spectrum, we have chosen the most important excited states. Indeed, we selected only those transitions which show an oscillator strength above a chosen threshold (2.5×10^{-2}). We remember that within the C_{2v} symmetry the dipole-allowed transitions belong to the A_1, B_1, and B_2 irreducible representations. The A_1 excitations have negligible intensity; therefore, we studied only the B_1 and B_2 transitions. See Figure 5 and Table 5 for further details.

Q Band. The calculated Q band of the planar Ni(oSHpz) complex is characterized mainly by three ligand-to-ligand charge transfer (LLCT) transitions: $2a_{1u} \rightarrow 7e_g$ (0.2084), $5a_{2u} \rightarrow 7e_g$ (0.2037), and $3b_{2u} \rightarrow 7e_g$ (0.0562). The numbers between parentheses are the squared coefficients of the single Slater determinants. These excitations have opposite transition dipole moments, and they tend to cancel out each other. The weights of these two contributions are almost the same; therefore, the total oscillator strength is small ($f = 0.0318$).

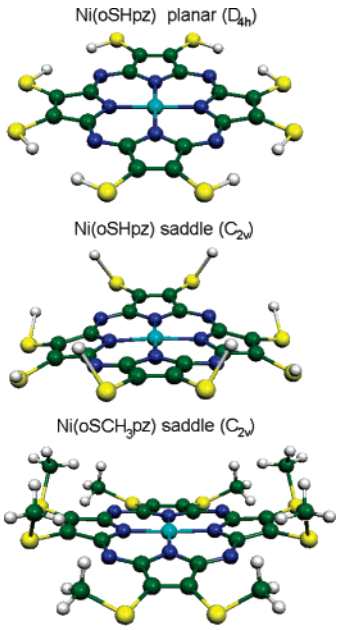

Figure 6. Conformations of Ni(oSXpz) [X = H, CH_3] complexes on which we performed TD−DFT calculations at the B3LYP/6-31g* level.

The ^1E_u excited states is downward-shifted toward lower energies with respect to the Ni(oCH$_3$pz) complex: from 2.48 eV (500 nm) to 2.13 eV (582 nm) at the B3LYP level (Figure 7). This effect is due to the decrease of both $5a_{2u}/7e_g$ and $3b_{2u}/7e_g$ gaps determined by the substitution of the peripheral CH_3 groups [Ni(oCH$_3$pz)] of the complex with the sulfur atoms [Ni(oSHpz)], as can be seen in Figure 3 [this figure represents the MO's energy levels calculated at the BP/TZ2P level: even if the absolute energy values are different, the trends between the Ni(oXHpz) complexes are similar to those obtained with the B3LYP/6-31g* approach]. In spite of a strong energy overestimation of the Q band for both the complexes, the difference between the excitation energies of the two peaks (82 nm) is in excellent agreement with the experimental one (83 nm).

The intensities of the computed Q bands are rather low with respect to the experiment (1.84 eV, 672 nm). Anyway, we can observe that in the case of the Ni(oSHpz) molecular distortion from the planar conformation to the saddled one an increase is provided of the oscillator strengths of these two bands, which lie closer to the experimental one. We remember that the structural deformation lowers the symmetry from D_{4h} to C_{2v}; therefore, the 1^1E_u excited state (Q band) is split in two into the 1^1B_1 and 1^1B_2 excitations. Indeed, also the composition of the Q band is slightly changed due to the geometry modification, and the 1^1B_1 and 1^1B_2 excitations are mainly formed by the $18a_2 \rightarrow 23b_2$ ($27a_1 \rightarrow 23b_1$) and $18a_2 \rightarrow 23b_1$ ($27a_1 \rightarrow 23b_2$) transitions, respectively, which correspond to the $3b_{2u} \rightarrow 7e_g$ and $2a_{1u} \rightarrow 7e_g$ ones in the planar D_{4h}. In the 1^1B_1 excitation, the weight of the $26a_1 \rightarrow 23b_1$ transition (which corresponds to the $5a_{2u} \rightarrow 7e_g$) is substantially smaller than the $18a_2 \rightarrow 23b_2$ ($f = 0.2867$); therefore, in spite of the opposite transition dipole moments, the oscillator strengths remains quite large ($f = 0.2186$). An analogous behavior is valid also for the 1^1B_2 excited state ($f = 0.1131$), which is characterized mainly by the $27a_1 \rightarrow 23b_2$ ($f = 0.4032$) transition. As concerns the excitation energies, the Q band is determined by a slight blue shift: from 586 nm (1^1E_u) to 566 nm (1^1B_1) and 535 nm (1^1B_2).

The further addition of methyl groups on the terminal sulfur atoms provides similar excitation energies (561 and 548 nm, respectively) for the 1^1B_1 and 1^1B_2 excited states and intense oscillator strengths ($f = 0.2627$ and 0.2749) in good agreement with the experimental Q band.

B Band. The extra band (2.45 eV; 506 nm) is composed mainly of the $5a_{2u} \rightarrow 7e_g$ (0.2371), $2a_{1u} \rightarrow 7e_g$ (0.1421), and $4a_{2u} \rightarrow 7e_g$ (0.0371) LLCT transitions. Previously,[64] this extra band was denoted as the W band because it was interpreted as a new band stemming from the substitution of the peripheral CH_3 groups with the sulfur atoms. From our point of view, on the basis of the composition of this excited state, we suggest that this band correspond to the B band of the [Ni(oCH$_3$pz)] complex, which is shifted to lower energies owing to the decrease of the $4a_{2u}/7e_g$ and $5a_{2u}/7e_g$ gaps. In this way, the Soret band of the Ni(oCH$_3$pz) molecule, composed by the three B, N, and L bands, which are enveloped in one wide band, is now decomposed and separated in different bands.

Moreover, the intensity of the computed B band seems to be too large for the experiment. In order to understand this last behavior, we analyzed the saddled Ni(oSHpz) complex, which provides an excitation energy of the B band similar to that obtained with the planar one. Indeed, the 2^1E_u (D_{4h}, planar) excited state (506 nm) is split into the more intense 2^1B_1 excitation (496 nm, $f = 0.1091$) and the less intense 2^1B_2 one (478 nm, $f = 0.0137$). The reduction of the oscillator strengths from $f = 0.4329$ (D_{4h}) is mainly due to the different contribution of the single Slater determinants involved in the transition. For instance, the composition of the 2^1B_1 excited state corresponds to the planar 2^1E_u one, but it is also mixed with a strong contribution from $25a_1 \rightarrow 23b_1$ (0.1098), which is present only in the saddled geometry. This transition quenches the oscillator strengths, which passes from 0.4329 (D_{4h}) to 0.1091 (C_{2v}). Furthermore, the 2^1B_1 excited state is characterized by the $25a_1 \rightarrow 23b_2$ (0.4191) transition and by marginal contributions from other transitions. In this way, this excitation has a small intensity. The distorted structure yields other allowed transition in the region between 430 and 500 nm, which can give important contributions to the experimental B band. In particular, two of them lie at 479 nm ($f = 0.0562$) and 443 nm ($f = 0.0810$).

The addition of the methyl groups in the Ni(oSCH$_3$pz) complex does not influence both the excitation energy (2^1B_1 502 nm and 2^1B_2 468 nm) and the oscillator strength (2^1B_1 0.1537 and 2^1B_2 0.0244) of the B band with respect to the saddled Ni(oSHpz) molecule. Furthermore, the two satellite peaks in the 430−500 nm region have negligible intensity and should be not crucial to the interpretation of the Ni(oSCH$_3$pz) spectrum.

N Band. The N band is the most intense of the entire spectrum. This characteristic is confirmed also by the strong oscillator strength ($f = 0.5578$). Besides, this 3^1E_u excited state lies at the same energy (309 nm) with respect to that obtained in the Ni(oCH$_3$pz) complex (310 nm). This excited

Table 5. Computed Vertical Excitation Energies (eV) and Oscillator Strengths of Different Ni(oSXpz) [X=H, CH3] Complexes at B3LYP/6-31g* Level

		composition	exp.	excitation energies eV (nm)	oscillator strength
SH	1 ^1E_u	0.2037($5a_{2u}\rightarrow 7e_g$); 0.0562($3b_{2u}\rightarrow 7e_g$); 0.2084($2a_{1u}\rightarrow 7e_g$)		2.13	0.0318
planar	(Q)			(582)	
SH	1 $^1B_1$	0.0580($27a_1\rightarrow 23b_1$); 0.2867($18a_2\rightarrow 23b_2$); 0.0209($24a_1\rightarrow 23b_1$)		2.19	0.2186
saddle				(566)	
	1 $^1B_2$	0.4032($27a_1\rightarrow 23b_2$); 0.0161($18a_2\rightarrow 23b_1$); 0.0236($24a_1\rightarrow 23b_2$)	1.84	2.32	0.1131
			(672)	(534)	
SCH_3	1 $^1B_1$	0.0369($27a_1\rightarrow 23b_1$); 0.3026($18a_2\rightarrow 23b_2$); 0.0271($24a_1\rightarrow 23b_1$)		2.21	0.2627
saddle				(561)	
	1 $^1B_2$	0.2537($27a_1\rightarrow 23b_2$); 0.1327($18a_2\rightarrow 23b_1$); 0.0268($24a_1\rightarrow 23b_2$)		2.26	0.2749
				(548)	
SH	2 ^1E_u	0.2371($5a_{2u}\rightarrow 7e_g$); 0.1421($2a_{1u}\rightarrow 7e_g$); 0.0371($4a_{2u}\rightarrow 7e_g$)		2.45	0.4329
planar	(B)			(506)	
SH	2 $^1B_1$	0.3128($26a_1\rightarrow 23b_1$); 0.0157($18a_2\rightarrow 23b_2$); 0.1098($25a_1\rightarrow 23b_1$)		2.50	0.1091
saddle				(496)	
	2 $^1B_2$	0.0289($26a_1\rightarrow 23b_2$); 0.1327($18a_2\rightarrow 23b_1$); 0.4191($25a_1\rightarrow 23b_2$)	2.56	2.59	0.0137
			(484)	(478)	
SCH_3	2 $^1B_1$	0.3904($26a_1\rightarrow 23b_1$); 0.0314($18a_2\rightarrow 23b_2$); 0.0155($25a_1\rightarrow 23b_1$)		2.47	0.1537
saddle				(502)	
	2 $^1B_2$	0.4046($26a_1\rightarrow 23b_2$); 0.0137($25a_1\rightarrow 23b_2$)		2.65	0.0244
				(468)	
SH	3 ^1E_u	0.2475($4a_{2u}\rightarrow 7e_g$); 0.1404($2b_{1u}\rightarrow 7e_g$); 0.0119($6e_g\rightarrow 3b_{1u}$); 0.0361($1a_{1u}\rightarrow 7e_g$)		4.01	0.5578
planar	(N)			(309)	
SH	3 $^1B_1$	0.2170($24a_1\rightarrow 23b_1$); 0.1227($22b_1\rightarrow 28a_1$); 0.0288($16a_2\rightarrow 23b_2$)		3.93	0.3569
saddle				(315)	
	3 $^1B_2$	0.0711($24a_1\rightarrow 23b_2$); 0.1660($22b_1\rightarrow 28a_1$); 0.1056($23a_1\rightarrow 23b_2$)	3.98	4.08	0.1555
			(311)	(304)	
SCH_3	3 $^1B_1$	0.1970($24a_1\rightarrow 23b_1$); 0.1427($22b_1\rightarrow 19a_2$); 0.0279($16a_2\rightarrow 23b_2$)		3.97	0.4713
saddle				(312)	
	3 $^1B_2$	0.0626($24a_1\rightarrow 23b_2$); 0.1546($22b_1\rightarrow 28a_1$); 0.1184($23a_1\rightarrow 23b_2$)		4.12	0.2089
				(301)	
SH	4 ^1E_u	0.4478($6e_g\rightarrow 3b_{1u}$); 0.0160($4a_{2u}\rightarrow 7e_g$)		3.69	0.0036
planar	(L)			(336)	
SH	4 $^1B_1$	0.2922($24a_1\rightarrow 23b_1$); 0.0614($22b_1\rightarrow 19a_2$)		3.85	0.3325
saddle				(322)	
	4 $^1B_2$	0.0644($24a_1\rightarrow 23b_2$); 0.3015($22b_1\rightarrow 28a_1$)	3.59	3.95	0.0111
			(345)	(314)	
SCH_3	4 $^1B_1$	0.2730($24a_1\rightarrow 23b_1$); 0.0814($22b_1\rightarrow 19a_2$)		3.82	0.3179
saddle				(324)	
	4 $^1B_2$	0.0666($24a_1\rightarrow 23b_2$); 0.3123($22b_1\rightarrow 28a_1$)		3.92	0.0073
				(316)	
SH	5 ^1E_u	0.3465($2b_{1u}\rightarrow 7e_g$); 0.0952($4a_{2u}\rightarrow 7e_g$); 0.0177($1a_{1u}\rightarrow 7e_g$)		4.07	0.0047
planar	(C)			(304)	
SH	5 $^1B_1$	0.3211($23a_1\rightarrow 23b_1$); 0.0812($22b_1\rightarrow 19a_2$)		4.00	0.0699
saddle				(310)	
	5 $^1B_2$	0.0994($23a_1\rightarrow 23b_2$); 0.3041($22b_1\rightarrow 28a_1$)		4.11	0.0085
				(301)	
SCH_3	5 $^1B_1$	0.3228($23a_1\rightarrow 23b_1$); 0.0915($22b_1\rightarrow 19a_2$)		4.05	0.0752
saddle				(306)	
	5 $^1B_2$	0.1004($23a_1\rightarrow 23b_2$); 0.2996($22b_1\rightarrow 28a_1$)		4.12	0.0112
				(301)	

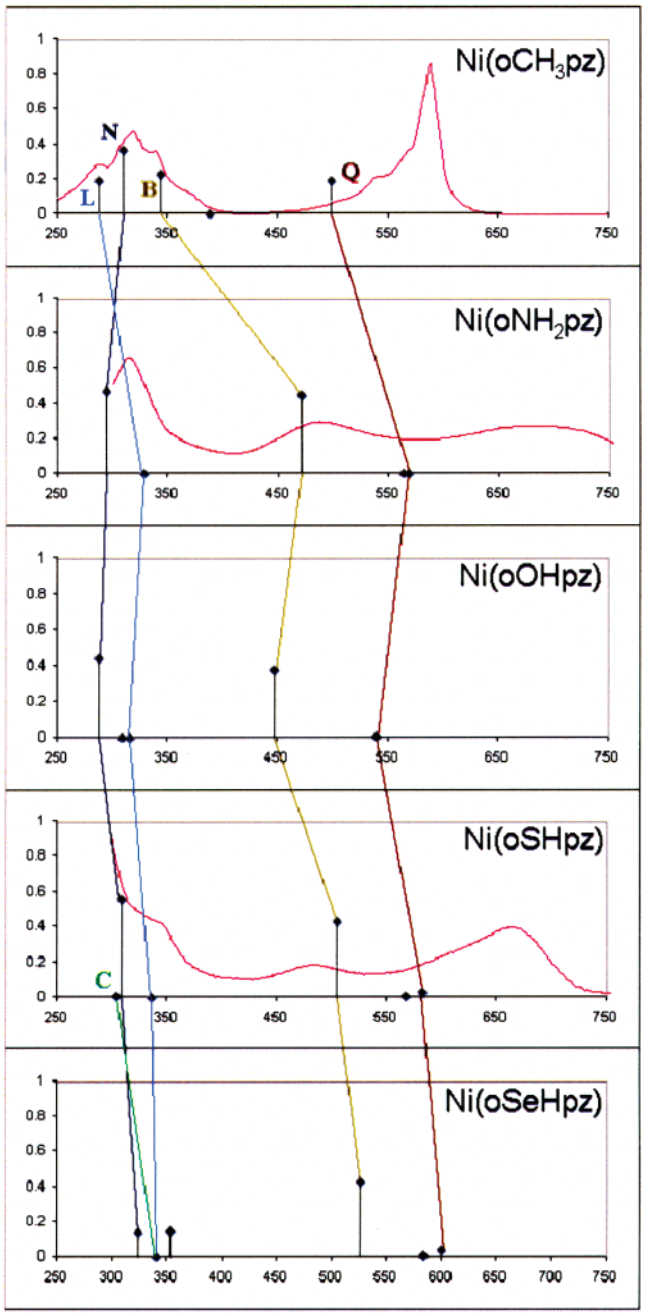

Figure 7. Vertical bold lines indicating the most important singlet−singlet excited states computed for the planar Ni(oXHpz) [X = CH_2, NH, O, S, Se] complexes at the B3LYP/6-31g* level. The available experimental spectra of the Ni(oEtpz),[9] Ni(oNMe$_2$pz),[32] and Ni(oSEtpz) complexes are indicated with continuum lines (—).

state is formed by the $4a_{2u} \rightarrow 7e_g$ (0.2475) and $1a_{1u} \rightarrow 7e_g$ (0.0361) transitions mixed with the $2b_{1u} \rightarrow 7e_g$ (0.1404) and $6e_g \rightarrow 3b_{1u}$ (0.0119) ones. Also in this case, transitions are mainly LLCTs with a small MLCT contribution provided by the $6e_g \rightarrow 3b_{1u}$ excitation. Indeed, the $6e_g$ MO is partially localized on the nickel ion (17%).

The saddled Ni(oSHpz) geometry induces a splitting of the 3^1E_u excited state into the 3^1B_1 and 3^1B_2. The former has a strong oscillator strength ($f = 0.3569$) and lies at 313 nm, while the latter is less intense ($f = 0.1555$) and is shifted to lower wavelengths (304 nm). The composition of these two bands is almost the same (only the weight of the single transition is changed) and corresponds to the N band in the case of the planar conformation (see Table 5).

The effect of the methyl groups on the sulfur atoms is not relevant. Indeed, the 3^1B_1 and 3^1B_2 excited states are determined by similar excitation energies (3^1B_1 312 nm; 3^1B_2 301 nm) and oscillator strengths (3^1B_1 $f = 0.4713$; 5^1B_2 $f = 0.2089$).

L Band. In the Ni(oCH$_3$pz) complex, the 4^1E_u excited state relative to the sh_3 shoulder is characterized mainly by the $6e_g \rightarrow 3b_{1u}$ MLCT transition and lies at higher energy than the N band. According to the labeling of Weiss at al.,[65] the sh_3 peak can be indicated using the L letter because at the B3LYP level this excited state is electronic in origin. Peripheral substitution with sulfur atoms determines a lowering of the $3b_{1u}$ MO energy and leaves the $6e_g$ MO energy substantially unaltered. Therefore, there is a decrease of the $6e_g/3b_{1u}$ gap, giving an excitation energy downward-shifted to lower energy (3.69 eV, 336 nm).

As in the previously described bands, also the 4^1E_u excited state is split into two transitions (4^1B_1 and 4^1B_2) owing to the lowering of the molecular symmetry from D_{4h} to C_{2v}. The 4^1B_1 excitation lies at 322 nm ($f = 0.3325$) and is more intense than the correspondent 4^1B_2 one (325 nm, $f = 0.0111$). The composition of these two bands presents a significant contribution from the $22b_1 \rightarrow 28a_1$ MLCT transition, which is equivalent to the $6e_g \rightarrow 3b_{1u}$ one of the planar complex.

The effect of adding the methyl terminal does not yield important variations with respect to the Ni(oSHpz) complex. For instance, the 4^1B_1 and 4^1B_2 excited states show similar excitation energies (4^1B_1 324 nm; 4^1B_2 316 nm) and oscillator strengths (4^1B_1 $f = 0.3179$; 4^1B_2 $f = 0.0073$).

C Band. Another interesting feature is based on the presence of one more transitions, denoted as the C band according to Weiss et al. labeling.[65] This excited state is mainly due to the $2b_{1u} \rightarrow 7e_g$ transition, and it falls to 4.07 eV (304 nm) with a low oscillator strength, that is, at a higher energy than the N band. When we perform the distortion from the planarity, the 5^1E_u excited state is split into the 5^1B_1 ($f = 0.0699$) and 5^1B_2 ($f = 0.0085$) transitions. In particular, the 5^1B_1 excitation has an oscillator strength smaller, on an order of 10, than the B band; thus, it can give a significant contribution to the widening of the Soret band. It is characterized manily by the $23a_1 \rightarrow 23b_1$ excitation, which corresponds to the $2b_{1u} \rightarrow 7e_g$ transition in the planar case.

Adding of the methyl groups on the sulfur atoms promotes the formation of 5^1B_1 and 5^1B_2 excited states, which have similar excitation energies (5^1B_1 306 nm; 5^1B_2 301 nm) and oscillator strengths (5^1B_1 $f = 0.0752$; 5^1B_2 $f = 0.0112$).

6.2. The CH_3, NH_2, and OH Peripheral Substitution Effect on the Trend of the Main Excited States. As we have seen in the previous section, the excitation energies of the main bands (Q, B, N, L, and C) calculated in the case of the planar Ni(oSHpz) conformation lie at similar energies to those obtained on the saddled Ni(oSCH$_3$pz) complex. Thus, in order to analyze the trend of the main excited states induced by the peripheral substitution, we performed calcula-

Table 6. Computed Vertical Excitation Energies (eV) and Oscillator Strengths of Different Ni(oXHpz) [X = CH_2, O, S, Se] (D_{4h}) and Ni(oNH2pz) (D_{2d}) Complexes at the B3LYP/6-31g* Level

state		composition	exp.	excitation energies eV (nm)	oscillator strength
1 ^1E_u	CH_3	0.0676($5a_{2u}\rightarrow 7e_g$); 0.0144($4a_{2u}\rightarrow 7e_g$); 0.0369($1a_{1u}\rightarrow 7e_g$)	2.11	2.48	0.1934
(Q)			(587)	(500)	
	NH_2	0.1514($13b_2\rightarrow 23e$); 0.1939($9a_2\rightarrow 23e$); 0.1205($10b_1\rightarrow 23e$)	wide band	2.18	0.0013
				(568)	
	OH	0.2362($5a_{2u}\rightarrow 7e_g$); 0.0100($4a_{2u}\rightarrow 7e_g$); 0.2201($2a_{1u}\rightarrow 7e_g$); 0.0254($3b_{2u}\rightarrow 7e_g$)		2.30	0.0096
				(539)	
	SH	0.2037($5a_{2u}\rightarrow 7e_g$); 0.0562($3b_{2u}\rightarrow 7e_g$); 0.2084($2a_{1u}\rightarrow 7e_g$);	1.84	2.13	0.0318
			(672)	(582)	
	SeH	0.0650($5a_{2u}\rightarrow 7e_g$); 0.2012($3b_{2u}\rightarrow 7e_g$); 0.2101($2a_{1u}\rightarrow 7e_g$);		2.06	0.0357
				(602)	
2 ^1E_u	CH_3	0.2746($5a_{2u}\rightarrow 7e_g$); 0.1745($4a_{2u}\rightarrow 7e_g$)	3.66	3.60	0.2297
(B)			(339)	(344)	
	NH_2	0.1492($13b_2\rightarrow 23e$); 0.1916($10b_1\rightarrow 23e$); 0.0510($12b_2\rightarrow 23e$)	2.53	2.63	0.4460
			(489)	(471)	
	OH	0.1880($5a_{2u}\rightarrow 7e_g$); 0.1486($2a_{1u}\rightarrow 7e_g$); 0.0564($4a_{2u}\rightarrow 7e_g$)		2.77	0.3761
				(447)	
	SH	0.2371($5a_{2u}\rightarrow 7e_g$); 0.1421($2a_{1u}\rightarrow 7e_g$); 0.0371($4a_{2u}\rightarrow 7e_g$)	2.56	2.45	0.4329
			(484)	(506)	
	SeH	0.2433($5a_{2u}\rightarrow 7e_g$); 0.1443($2a_{1u}\rightarrow 7e_g$); 0.0264($4a_{2u}\rightarrow 7e_g$)		2.36	0.4299
				(525)	
3 ^1E_u	CH_3	0.2209($4a_{2u}\rightarrow 7e_g$); 0.0961($5a_{2u}\rightarrow 7e_g$); 0.0576($6e_g\rightarrow 3b_{1u}$); 0.0144($1a_{1u}\rightarrow 7e_g$)	3.92	4.09	0.3689
(N)			(316)	(303)	
	NH_2	0.3418($12b_2\rightarrow 23e$); 0.0145($22e\rightarrow 3b_{1u}$)	3.91	4.22	0.4715
			(317)	(294)	
	OH	0.2209($4a_{2u}\rightarrow 7e_g$);0.0576($6e_g\rightarrow 3b_{1u}$)		4.30	0.4420
				(288)	
	SH	0.2475($4a_{2u}\rightarrow 7e_g$); 0.1404($2b_{1u}\rightarrow 7e_g$); 0.0119($6e_g\rightarrow 3b_{1u}$); 0.0361($1a_{1u}\rightarrow 7e_g$)	3.98	4.01	0.5578
			(311)	(309)	
	SeH	0.1690($4a_{2u}\rightarrow 7e_g$);0.0371($6e_g\rightarrow 3b_{1u}$); 0.2749($1a_{1u}\rightarrow 7e_g$)		3.82	0.1391
				(324)	
4 ^1E_u	CH_3	0.4225($6e_g\rightarrow 3b_{1u}$); 0.0324($5a_{2u}\rightarrow 7e_g$)	4.27	4.31	0.1933
(L)			(290)	(288)	
	NH_2	0.4527($22e\rightarrow 3b_{1u}$); 0.0171($12b_2\rightarrow 23e$)		3.77	0.0020
				(329)	
	OH	0.4319($6e_g\rightarrow 3b_{1u}$); 0.0200($4a_{2u}\rightarrow 7e_g$)		3.93	0.0006
				(315)	
	SH	0.4478($6e_g\rightarrow 3b_{1u}$); 0.0160($4a_{2u}\rightarrow 7e_g$)	3.59	3.69	0.0036
			(345)	(336)	
	SeH	0.4320($6e_g\rightarrow 3b_{1u}$); 0.0330($4a_{2u}\rightarrow 7e_g$)		3.64	0.0023
				(340)	
5 ^1E_u	CH_3	Over 4.30 eV			
(C)	NH_2	Over 4.30 eV			
	OH	Over 4.30 eV			
	SH	0.3465($2b_{1u}\rightarrow 7e_g$); 0.0952($4a_{2u}\rightarrow 7e_g$); 0.0177($1a_{1u}\rightarrow 7e_g$)		4.07	0.0047
				(304)	
	SeH	0.4844($2b_{1u}\rightarrow 7e_g$)		3.51	0.1455
				(353)	

tions on the less crowded planar complexes. We remember that the Ni(oNH$_2$pz) complex belongs to the D_{2d} point group, whereas the Ni(oOHpz) and Ni(oCH$_3$pz) have D_{4h} symmetry. Furthermore, we can perform a comparison between the calculated data and the experimental ones owing to the presence of spectra collected on the Ni(oEtpz)[47] and Ni(oNH$_2$pz)[62] complexes. See Figure 7 and Table 6 for further details.

Along the CH$_3$ and NH$_2$ series, the Q band is downward-shifted to lower energies from 2.48 eV (500 nm) to 2.18 eV (569 nm). This effect is mainly due to the strong contraction of the 13b$_2$/23e and 9a$_2$/23e gaps induced by the peripheral introduction of amine groups (see also Figure 3). We remember that the 13b$_2$, 9a$_2$, and 23e (D_{2d}) correlate respectively to 5a$_{2u}$, 3b$_{2u}$, and 7e$_g$ (D_{4h}). The shift of the Q band is also visible in the experimental spectra, in which the Q band is red-shifted by about 100 nm. As regards the Ni(oOHpz) complex, the Q band is situated at lower energy (2.30 eV, 539 nm) than the respective one of the Ni(oCH$_3$-pz) molecule but is slightly blue-shifted (∼20 nm) with respect to the Ni(oNH$_2$pz) complex.

The B band involves the same transitions of the Q band but with a stronger contribution from the 4a$_{2u}$ → 7e$_g$ excitation. Also in this case, the contraction of the 13b$_2$/23e gap provides a red shift of about 130 nm. This effect is observable in the experimental spectra: the B band lies in the visible region of the Ni(oNH$_2$pz) spectrum, whereas it represents a shoulder of the Soret band in the Ni(oCH$_3$pz) spectrum. The experimental displacement of these two bands (∼150 nm) is therefore well-described by the calculations (130 nm). Furthermore, the Ni(oOHpz) complex promotes the B band at 2.77 eV (447 nm), that is, at lower energy than the Ni(oCH$_3$pz) but at higher energy than the Ni(oNH$_2$-pz) complex.

The N band is composed mainly of the 4a$_{2u}$ → 7e$_g$ (12b$_2$ → 23e) transition, and its relative gap does not change significantly along the CH$_3$, NH$_2$, and OH series (see Figure 3). Calculations suggest a small blue shift of the N band, but this effect is not visible in the experimental spectra owing to the presence of wide bands, which do not allow to pinpoint the shift on the order of 10−20 nm.

As concerns the L band, we can observe a red shift of 41 nm along the C and N series owing to the contraction of the 22e/14a$_1$ (6e$_g$/3b$_{1u}$) gap. This effect determines a displacement of this band, which passes from the left (higher energy) to the right (lower energy) of the N band. This characteristic is also found for the complex with terminal oxygen atoms, but the shifting is less intense (∼28 nm).

6.3. The OH, SH, and SeH Peripheral Substitution Effect on the Trend of the Main Excited States. No experimental UV−vis spectra are available for the Ni(oOHpz) and Ni(oSeHpz) molecules; hence, our analysis is based on the possible changes in the energy and in the oscillator strengths of the excited states owing to the peripheral substitution with different chalcogen atoms (Figure 7).

The ^{1}E$_u$ excited states, related to the Q band, show a decrease of the excitation energy along the chalcogen series: from 2.30 eV (539 nm) (X = O) to 2.06 eV (602 nm) (X = Se). This stems from the monotonic contraction of the 5a$_{2u}$/7e$_g$ and 3b$_{2u}$/7e$_g$ gaps (Figure 3). Also, the oscillator strengths are similar, with the exception of the Q transition of Ni(oOHpz), which is less intense than the corresponding one of the Ni(oSHpz) and Ni(oSeHpz) complexes. The other excited states show a similar trend for the B, L, N, and C bands. In particular, the C band, which lies at much higher energy than the N band along the CH$_3$, NH$_2$, and OH series (over 4.30 eV; 288 nm), is significantly shifted toward lower energy: 4.07 eV (304 nm) for Ni(oSHpz) and 3.51 eV (353 nm). This effect is due to the different behavior of the 2b$_{1u}$ MO in the Ni(oXHpz) [x = O, S, Se] complexes. Indeed, as can be seen in the ground-state section and in Figure 3, the 2b$_{1u}$ MO is upward-shifted to less negative energies, providing a strong decrease of the 2b$_{1u}$/7e$_g$ gaps along the chalcogen series. This effect determines a lowering of the excitation energy. This characteristic is particularly important for the interpretation of the differences between the experimental Soret bands of the Ni(oNMe$_2$pz) and Ni(oSEtpz) compounds. Indeed, in Figure 7 we can observe a larger intensity for the complex with terminal sulfur atoms. From our calculations, the N and the L bands of the Ni(oNH$_2$pz) and Ni(oSHpz) molecules lie at almost the same excitation energies and oscillator strengths. Therefore, the higher intensity of the Ni(oSHpz) Soret band can be attributed to the presence of the C band, which adds its contribution to the total intensity of the Soret band.

7. Conclusions

Density functional calculations allow characterization of the molecular and electronic structure of the ground state of Ni(oXHpz) [X = O, S, Se, CH$_2$] complexes. The peripheral substitution has an effect on the MO energy levels. In particular, the molecules with a methyl terminal group present the highest HOMO and LUMO energies and the most negative bonding energy between the metal ion and the macrocycle fragment, while the molecules with sulfur atoms have the lowest HOMO and LUMO energies, and the molecules with selenium atoms present the highest bonding energy.

The peripheral substituents cause modifications to the "core" properties of the macrocycle, changing σ and π interactions between the metal ion and the dianion fragment. Peripherally unhindered Ni(oXHpz) complexes are all planar because Ni−N$_p$ distances are all above the threshold for ruffling. The largest contribution to the bonding energy is the total orbital interactions, which is larger than the ionic contribution throughout the series of all the complexes. The orbital interactions are based mainly on a σ donation from the nitrogen lone pairs to the $d_{x^2-y^2}$ orbital of the metal. Furthermore, there is a consistent flow of charge from σ macrocyclic orbitals to Ni-4p$_\sigma$ (e$_u$); the π interactions are weaker but also important: a back-donation from Ni-3d$_\pi$ (e$_g$) to the empty π "cage" orbitals is present.

TD−DFT calculations allow analysis of the excited states of Ni(oXHpz), and we have compared theoretical results with available experimental spectra [Ni(oEtpz), Ni(oSEtpz), and Ni(N Me$_2$pz)]. On the basis of the calculated and the experimental data, we can conclude that the Ni(oCH$_3$pz)

spectrum shows two main bands: the Q band and the broad Soret band, which is composed of three secondary peaks, denoted as B, N, and L. The peripheral substitution with chalcogen, carbon, and nitrogen atoms determines the decomposition of the Soret band into separate peaks: for example, the B band is shifted to lower energies, while the N and L peaks yield one single band. Moreover, the C band, which lies at energies over 4.30 eV (288 nm) along the C, N, O series, is downward-shifted to lower energies due to the terminal substitution with sulfur and selenium atoms. In the Ni(oSHpz) complex, the C peak is close to the N and L peaks to form the Soret band, as observed in the experimental Ni(oSEtpz) spectrum. According to the calculations, in an eventual Ni(oSeHpz) UV−vis spectrum, the C band should lie as a separate band between the Soret and B bands.

Experimental and theoretical chemical "perturbation" of the reference molecule Ni(oCH3pz) by peripheral substitution allows one to track and follow the modification of the computed and measured spectra giving a more firmly grounded interpretation of the properties of this interesting class of molecules.

The same approach we have seen before can be used to analyze the properties determined of the metal substitution with the first row of transition elements. These properties can allow us then to point out the reactivity of these compounds.

Acknowledgment. Financial support through MIUR grants within "legge 488 − cluster 14 po.5 e cluster 16 po.8" and from the Laboratorio per la Sintesi e la Caratterizzazione dei Materiali Molecolari (LASCAMM) of INSTM Sezione Basilicata is gratefully acknowledged. Thanks are expressed to Prof. Ricciardi for collecting the UV−vis spectrum for Ni(oSEtpz).

References

(1) Hoffman, B. M.; Barrett, A. G. M. Heteroatom-Functionalized Porphyrazines and Multimetallic Complexes and Polymers Derived Therefrom. U.S. Patent 5,912,341, 1999.

(2) Andersen, K.; Anderson, M.; Anderson, O. P.; Baum, S.; Baumann, T. F.; Beall, L. S.; Broderick, W. E.; Cook, A. S.; Eichhorn, D. M.; Goldberg, D.; Hope, H.; Jarrell, W.; Lange, S. J.; McCubbin, Q. J.; Mani, N. S.; Miller, T.; Montalban, A. G.; Rodriguez-Morgade, M. S.; Lee, S.; Nie, H.; Olmstead, M. M.; Sabat, M.; Sibert, J. W.; Stern, C.; White, A. J. P.; Williams, D. B. G.; Williams, D. J.; Barrett, A. G. M.; Hoffman, B. M. *J. Heterocycl. Chem.* **1998**, *35* (5), 1013−1042.

(3) Bahr, G.; Schleiter, G. *Chem. Ber.* **1957**, *90*, 438.

(4) Deng, K. M.; Ding, Z. N.; Ellis, D. E.; Michel, S. L. J.; Hoffman, B. M. *Inorg. Chem.* **2001**, *40* (6), 1110−1115.

(5) Ehrlich, L. A.; Skrdla, P. J.; Jarrell, W. K.; Sibert, J. W.; Armstrong, N. R.; Saavedra, S. S.; Barrett, A. G. M.; Hoffman, B. M. *Inorg. Chem.* **2000**, *39* (18), 3963−3969.

(6) Fitzgerald, J.; Haggerty, B. S.; Rheingold, A. N.; May, L. *Inorg. Chem.* **1992**, *31*, 2006.

(7) Fuchter, M. J.; Beall, L. S.; Baum, S. M.; Montalban, A. G.; Sakellariou, E. G.; Mani, N. S.; Miller, T.; Vesper, B. J.; White, A. J. P.; Williams, D. J.; Barrett, A. G. M.; Hoffman, B. M. *Tetrahedron* **2005**, *61* (25), 6115−6130.

(8) Ghosh, A.; Fitzgerald, J.; Gassman, P. G.; Almolof, J. *Inorg. Chem.* **1994**, *33*, 6057.

(9) Hochmuth, D. H.; Michel, S. L. J.; White, A. J. P.; Williams, D. J.; Barrett, A. G. M.; Hoffman, B. M. *Eur. J. Inorg. Chem.* **2000**, *4*, 593−596.

(10) Kandaz, M.; Michel, S. L. J.; Hoffman, B. M. *J. Porphyrins Phthalocyanines* **2003**, *7* (9−10), 700−712.

(11) Lee, S. W.; White, A. J. P.; Williams, D. J.; Barrett, A. G. M.; Hoffman, B. M. *J. Org. Chem.* **2001**, *66* (2), 461−465.

(12) Michel, S. L. J.; Barrett, A. G. M.; Hoffman, B. M. *Inorg. Chem.* **2003**, *42* (3), 814−820.

(13) Michel, S. L. J.; Hoffman, B. M.; Baum, S. M.; Barrett, A. G. M. Peripherally Functionalized Porphyrazines: Novel Metallomacrocycles with Broad, Untapped Potential. *Prog. Inorg. Chem.* **2001**, *50*, 473−590.

(14) Montalban, A. G.; Jarrell, W.; Riguet, E.; McCubbin, Q. J.; Anderson, M. E.; White, A. J. P.; Williams, D. J.; Barrett, A. G. M.; Hoffman, B. M. *J. Org. Chem.* **2000**, *65* (8), 2472−2478.

(15) Montalban, A. G.; Meunier, H. G.; Ostler, R. B.; Barrett, A. G. M.; Hoffman, B. M.; Rumbles, G. *J. Phys. Chem. A.* **1999**, *103* (22), 4352−4358.

(16) Schramm, C. J.; Hoffman, B. M. *Inorg. Chem.* **1980**, *19*, 383.

(17) Velàzquez, C. S.; Fox, G. A.; Broderick, E.; Andersen, K. A.; Anderson, O. P.; Barrett, A. G. M.; Hoffman, B. M. *J. Am. Chem. Soc.* **1992**, *114*, 7416.

(18) Vesper, B. J.; Lee, S.; Hammer, N. D.; Elseth, K. M.; Barrett, A. G. M.; Hoffman, B. M.; Radosevich, J. A. *J. Photochem. Photobiol., B* **2006**, *82* (3), 180−186.

(19) Vesper, B. J.; Lee, S. W.; Barrett, A. G. M.; Hoffman, B. M. *Abstr. Pap.−Am. Chem. Soc.* **2001**, *222*, U563−U563.

(20) Yaping, N.; Fitzgerald, J.; Carroll, P.; Wayland, B. B. *Inorg. Chem.* **1994**, *33*, 2029.

(21) Zhao, M.; Stern, C.; Barrett, A. G. M.; Hoffman, B. M. *Angew. Chem., Int. Ed.* **2003**, *42* (4), 462+.

(22) Ricciardi, G.; Bencini, A.; Ciofini, I.; Rosa, A. *Inorg. Chem.* **1999**, *38*, 1422.

(23) Ricciardi, G.; Belviso, S.; Bencini, A.; Bavoso, A.; Lelj, F. *J. Chem. Soc., Dalton Trans.* **1998**, 1985.

(24) Ricciardi, G.; Bencini, A.; Bavoso, A.; Rosa, A.; Lelj, F. *J. Chem. Soc., Dalton Trans.* **1996**, 3243.

(25) Ricciardi, G.; Bencini, A.; Bavoso, A.; Rosa, A.; Lelj, F. *J. Chem. Soc., Dalton Trans.* **1996**, 2799.

(26) Bonosi, F.; Ricciardi, G.; Lelj, F.; Martini, G. *Thin Solid Films* **1994**, *243*, 310.

(27) Bonosi, F.; Ricciardi, G.; Lelj, F.; Martini, G. *J. Phys. Chem* **1994**, *98*, 10613.

(28) Bonosi, F.; Ricciardi, G.; Lelj, F.; Martini, G. *J. Phys. Chem* **1993**, *97*, 9181.

(29) Lelj, F.; Morelli, G.; Ricciardi, G.; Roviello, A.; Sirigu, A. *Liq. Cryst.* **1992**, *12* (6), 941.

(30) Morelli, G.; Ricciardi, G.; Roviello, A. *Chem. Phys. Lett.* **1991**, *185*, 468.

(31) Ricciardi, G.; Lelj, F.; Bonosi, F. *Thin Solid Films* **1994**, *243*, 310.

(32) Ricciardi, G.; Lelj, F.; Bonosi, F. *J. Phys. Chem* **1993**, *215*, 541.

(33) Belviso, S.; Ricciardi, G.; Lelj, F.; Scolaro, L. M.; Bencini, A.; Carbonera, C. *J. Chem. Soc., Dalton Trans.* **2001**, 1143.

(34) LeCours, S. M.; Guan, H. W.; Di Magno, S. G.; Wang, C. H.; Therien, M. J. *J. Am. Chem. Soc.* **1996**, *118*, 1497.

(35) Priyadarshy, S.; Therien, M. J.; Beratan, D. N. *J. Am. Chem. Soc.* **1996**, *118*, 1504.

(36) Scheidt, W. R. *The Porphyrin Handbook*; Kadish, K. M., Smith, K. M., Guilard, R., Eds.; PUBLISHER: New York, 2000; Vol. 3, pp 49−112.

(37) Scheidt, W. R.; Lee, Y. J. *Struct. Bonding (Berlin, Ger.)* **1987**, *64*, 2.

(38) Shelnutt, J. A. *The Porphyrin Handbook*; Kadish, K. M., Smith, K. M., Guilard, R., Eds.; PUBLISHER: New York, 2000; Vol. 7, pp 167−223.

(39) Shelnutt, J. A.; Song, X. Z.; Ma, J. G.; Jia, S. L.; Jentzen, W.; Medforth, C. J. *Chem. Soc. Rev.* **1998**, *27*, 31.

(40) Ghosh, A.; Vangberg, T. *J. Am. Chem. Soc.* **1999**, *121*, 12154.

(41) Gouterman, M. *J. Chem. Phys.* **1959**, *30*, 1139.

(42) Ziegler, T.; Rauk, A. *Theor. Chim. Acta* **1977**, *46*, 1.

(43) Ziegler, T.; Rauk, A. *Inorg. Chem.* **1979**, *18*, 1558.

(44) Ziegler, T.; Tschinke, V.; Becke, A. *J. Am. Chem. Soc.* **1987**, *109*, 1351.

(45) Ziegler, T.; Tschinke, V.; Ursenbach, C. *J. Am. Chem. Soc.* **1987**, *109*, 4825.

(46) Ziegler, T.; Tschinke, V.; Versluis, L.; Baerends, E. J. *Polyhedron* **1988**, *7*, 1625.

(47) Rosa, A.; Ricciardi, G.; Baerends, E. J.; van Gisbergen, S. J. A. *J. Phys. Chem. A* **2001**, *105*, 3311.

(48) van Gisbergen, S. J. A.; Rosa, A.; Ricciardi, G. *J. Chem. Phys.* **1999**, *111*, 2499.

(49) Infante, I.; Lelj, F. *Chem. Phys. Lett.* **2003**, *367*, 308.

(50) Parr, R. G.; Yang, W. *Density Functional Theory of Atoms and Molecules*; PUBLISHER: New York, 1989.

(51) Becke, A. D. *J. Chem. Phys.* **1993**, *398*, 5648.

(52) Frisch, M. J.; Trucks, G. W.; Schlegel, H. B.; Scuseria, G. E.; Robb, M. A.; Cheeseman, J. R.; Zakrzewski, V. G.; Montgomery, J. A.; Stratmann, R. E.; Burant, J. C.; Dapprich, S.; Millam, J. M.; Daniels, A. D.; Kudin, K. N.; Strain, M. C.; Farkas, O.; Tomasi, J.; Barone, V.; Cossi, M.; Cammi, R.; Mennucci, B.; Pomelli, C.; Adamo, C.; Clifford, S.; Ochterski, J.; Petersson, G. A.; Ayala, P. Y.; Cui, Q.; Morokuma, K.; Malick, D. K.; Rabuck, A. D.; Raghavachari, K.; Foresman, J. B.; Cioslowski, J.; Ortiz, J. V.; Stefanov, B. B.; Liu, G.; Liashenko, A.; Piskorz, P.; Komaromi, I.; Gomperts, R.; Martin, R. L.; Fox, D. J.; Keith, T.; Al-Laham, M. A.; Peng, C. Y.; Nanayakkara, A.; Gonzalez, C.; Challacombe, M.; Gill, P. M. W.; Johnson, B. G.; Chen, W.; Wong, M. W.; Andres, J. L.; Head-Gordon, M.; Replogle, E. S.; Pople, J. A. *Gaussian 98*; Gaussian, Inc.: Pittsburgh, PA, 1998.

(53) Baerends, E. J.; Ellis, D. E.; Ros, P. *Chem. Phys.* **1973**, *2*, 42.

(54) Fonseca Guerra, C.; Snijders, J. G.; te Velde, G.; Baerends, E. J. *Theor. Chem. Acc.* **1998**, *99*, 391.

(55) te Velde, G.; Baerends, E. J. *J. Comput. Phys.* **1992**, *99*, 84.

(56) Perdew, J. P. *Phys. Rev. B: Condens. Matter Mater. Phys.* **1986**, *33*, 8822.

(57) Casida, M. E. *Recent Developments and Applications of Modern Density Func.*; Elsevier: Amsterdam, 1996; Vol. 4.

(58) Casida, M. E.; Chong, D. P. *Recent Advances in Density Functional Methods*; World Scientific: Singapore, 1995; Vol. 1, p 155.

(59) Davidson, E. R. *J. Comput. Phys.* **1975**, *17*, 87.

(60) Stratmann, R. E.; Scuseria, G. E.; Frisch, M. J. *J. Chem. Phys.* **1998**, *109*, 8218.

(61) Nguyen, K. A.; Day, P. N.; Pachter, R. *J. Chem. Phys.* **1999**, *110*, 9135.

(62) Goldberg, D. P.; Montalban, A. G.; White, A. J. P.; Williams, D. J.; Barrett, A. G. M.; Hoffman, B. M. *Inorg. Chem.* **1998**, *37*, 2873.

(63) Gouterman, M. *Porphyrins*; Dolphin, D., Ed.; Academic: New York, 1978; Vol. II.

(64) Guo, L.; Ellis, D. E.; Hoffman, B. M.; Ishikawa, Y. *Inorg. Chem.* **1996**, *35*, 5304.

(65) Weiss, C.; Kobayashi, H. M. G. *J. Mol. Spectrosc.* **1965**, *16*, 415.

CT6003609